Growth and Form of Rippled Icicles

Menno Demmenie,[1,2,*] Lars Reus,[1] Paul Kolpakov,[1] Sander Woutersen,[2] Daniel Bonn,[1] and Noushine Shahidzadeh[1]

[1] *Institute of Physics, University of Amsterdam, Science Park 904, Amsterdam 1098 XH, Netherlands*

[2] *Van 't Hoff Institute for Molecular Sciences, University of Amsterdam, Science Park 904, Amsterdam 1098XH, Netherlands*

(Received 16 September 2022; revised 15 December 2022; accepted 15 December 2022; published 2 February 2023)

Icicles are known for their universal conelike shape and rippled surface, and for both these features theories have been developed. However, experimental results appear to be at odds with the existing theories: for pure water in fact very irregular icicles are observed, and it is only if some salt is present that the cone shape and the surface ripples are observed. Here, we investigate the effect of such impurities on the morphology of icicles. We observe surface ripples with a wavelength of approximately equal to 1 cm that is independent of impurity concentration. Surprisingly, the amplitude of the ripples is zero for ultrapure water and increases rather sharply with impurity concentration. We find that the expulsion of salt from the ice crystal leads to a transition between partial to complete wetting of the water on the icicle, and it is only for the latter case that the icicles become well behaved. This is confirmed by adding a small amount of dye to the water that has different color in the liquid and solid phase, and image the growing icicles. These experiments show that in the presence of impurities in the water (causing complete wetting), the icicles are covered with a thin liquid film that speeds up icicle and ripple growth. In contrast, icicles grown from ultrapure water exhibit partial wetting, and grow due to droplets sliding down in stick-slip motion, leading to an ill-defined overall shape that differs from the theoretically predicted one, and a disappearance of the ripples.

DOI: 10.1103/PhysRevApplied.19.024005

I. INTRODUCTION

Icicles are formed when a gravity-driven flow of water slowly solidifies on its own crystal surface [1–6]. The freezing process produces latent heat that is carried away to the liquid-air interface by convection and subsequently released into the air. Since heat is dissipated most efficiently at the tip, icicles grow faster in the vertical direction than in the radial direction, resulting in the familiar pointed shape. A previous study by Short *et al.* examined icicle formation as a free-boundary problem, and predicted that icicles grow into a universal, conelike shape [7]. However, extensive experimental work by Morris *et al*. reveals icicles in a wide variety of shapes, apparently contradicting the predicted universal shape [8,9]. Moreover, in the most recent work they demonstrated, with the addition of sodium fluorescent, that the liquid flow over icicles is a complex stochastic system, where ionic solutes contribute positively to the wetting of icicles. As a consequence, the addition of ionic impurities resulted in circumferential ripple formation with a wavelength of approximately 1 cm, in agreement with commonly observed ripples on natural icicles [Fig. 1(a)], and with earlier studies [10].

In 1964 Mullins and Sekerka published a general model for morphological instabilities caused by a solidification front [11]. A protrusion at the interface causes enhanced thermal diffusion, and thus faster crystallization. Reduction of the local melting temperature because of the Gibbs-Thomson effect acts against bump growth. In the case of a thin water film on ice, this balance leads to a rippled surface with a wavelength of hundreds of micrometers [12,13]. To explain why icicles typically exhibit ribs that are 100 times larger, Ueno *et al.* [2] suggest that ripples form due to an underlying instability that can be described theoretically. In short, the model is based on a small perturbative expansion, in the form of an amplified wave, of the solid-liquid interface of an icicle. Gravity and surface tension both act as restoring forces, opposing the rippled pattern at the liquid-air interface. Hence, a complex disturbance of the heat flux emerges in the gravity-driven liquid layer, since the latent heat from the concave area has to migrate a longer distance towards the liquid-air interface than the latent heat coming from the convex area, as shown in Fig. 1(b). As a result, ripples with a wavelength of approximately 1 cm undergo maximum amplification

*M.demmenie@uva.nl

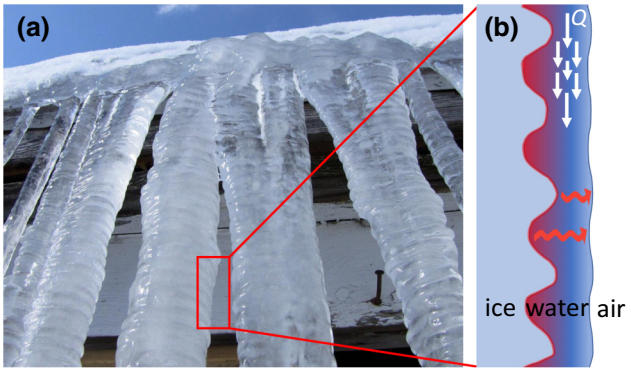

FIG. 1. (a) Typical icicles found in nature (photo by K. Purdy). (b) Schematic representation of the ripple growth theory proposed by Ueno [2], with ice on the left and air on the right. A perturbative expansion is chosen to be an amplified wave at the solid-liquid interface. Both gravity and surface tension oppose this morphology on the liquid-air interface. Therefore the latent heat (depicted by curved red arrows) from the concave areas has a longer convection distance before it is released in the air than the latent heat of the convex area. The combination with gravity-driven flow (Q) causes a complex disturbance of the heat flux, resulting in an instability that produces ripples with a wavelength of approximately 1 cm.

at the solid-liquid interface, and this explains the commonly observed ribs on icicles. However, the presence of ionic solutes as condition for ripple formation observed by Morris *et al.* seems difficult to explain with this theory. Moreover, the analysis of Ueno *et al*. requires *ad hoc* boundary conditions for which uniform coverage of a thin liquid film is assumed. Hence, wettability of the icicle is a key factor in ripple formation, as shown in this study.

To investigate why ionic impurities are necessary for the formation of icicles with the ribs and overall shape predicted by theory, we here study the growth and form of lab-grown icicles with varying concentrations of NaCl and other solutes. First we focus on the predicted universal shape [7], then on the surface ripples, and investigate why impurities seem to be essential for both these morphological aspects. We find that the presence of small concentrations of salt enhances the wetting of the ice surface tremendously, and we argue that this explains the observed dependence of the overall shape and the ripples on the presence or absence of impurities in the water.

II. EXPERIMENTAL DETAILS

Measurements are carried out in a climate chamber (KWP 240 Weiss) with a built-in temperature control system (Eurotherm 2404) that is set to an ambient temperature of -15°C. The water supply is regulated by a syringe pump (Thermo Orion Sage m362) with a capacity of three syringes of 60 ml. The syringe pump is positioned outside the climate chamber to prevent freezing, with water entering the chamber via a Teflon tube. To prevent the water inside this tube from freezing it is accompanied by an external neighboring flow of warm water with a temperature of 36°C (ThermoFisher Haake A25). The temperature of the released water is measured by a Voltcraft PL-125-T2USB VS temperature probe, and had a typical value of approximately 15°C.

The outlet of the tube is placed 5 cm above a fixed cone-shaped mesh with a spacing of 2 mm. Therefore, the water is randomly distributed radially along the icicle. To initiate crystallization, the flow is slowly built up to a final rate of 60 ml/h. At the back of the climate chamber a light-emitting diode (LED) panel illuminated the icicles for better contrast. A schematic overview of the setup can be found within the Supplemental Material (Fig. S5) [14]. Each minute an image is taken using a Nikon D5200 digital camera to generate a time lapse of the growth. Contour plots are extracted from the photographs using the Python OpenCV cv2 software.

To investigate to what extent wetting is enhanced by adding NaCl, sessile droplet experiments are conducted with an Easydrop Kruss GmbH in a humidity-controlled environment. The humidity is regulated by a steady flow of dry nitrogen and monitored by a thermometer or hygrometer (Testo 645). The droplets are illuminated by an external light source from the top to enhance contrast. Ice layers are formed on top of a copper plate ($560 \times 380 \times 40$ mm) to minimize temperature variations within the layer. Ice temperatures down to -10°C are achieved by a Peltier element (connected to BaseTech BT-305), which is placed underneath the copper plate and treated with thermal grease. Droplets of 8 μl are brought into contact with the ice layer by moving the stage upwards with a velocity of approximately 0.5 mm/s. Hence, droplet spreading because of the nonzero impact velocity can be minimized. Experiments on both icicles and sessile droplets are conducted using ultrapurified water from a Milli-Q system with the addition of NaCl (Sigma Aldrich 99,95%) or Sucrose (Sigma Aldrich) to induce impurities. We use conductivity measurements to calculate the salt concentration of purified Milli-Q water: 5.6×10^{-6} M.

III. RESULTS AND DISCUSSION

Figure 2 shows typical icicles formed from water with different concentrations of NaCl. With increasing salt concentration, we find that icicles become more opaque, the icicle surface becomes less smooth, exhibiting clear ripple formation, and the total icicle volume increases, indicating enhanced crystallization rates. From series of such photographs, we determine the maximum width close to the base W and overall length L of each icicle as it grows as a function of time t, as shown in Figs. S1 and S2 within the Supplemental Material, respectively [15].

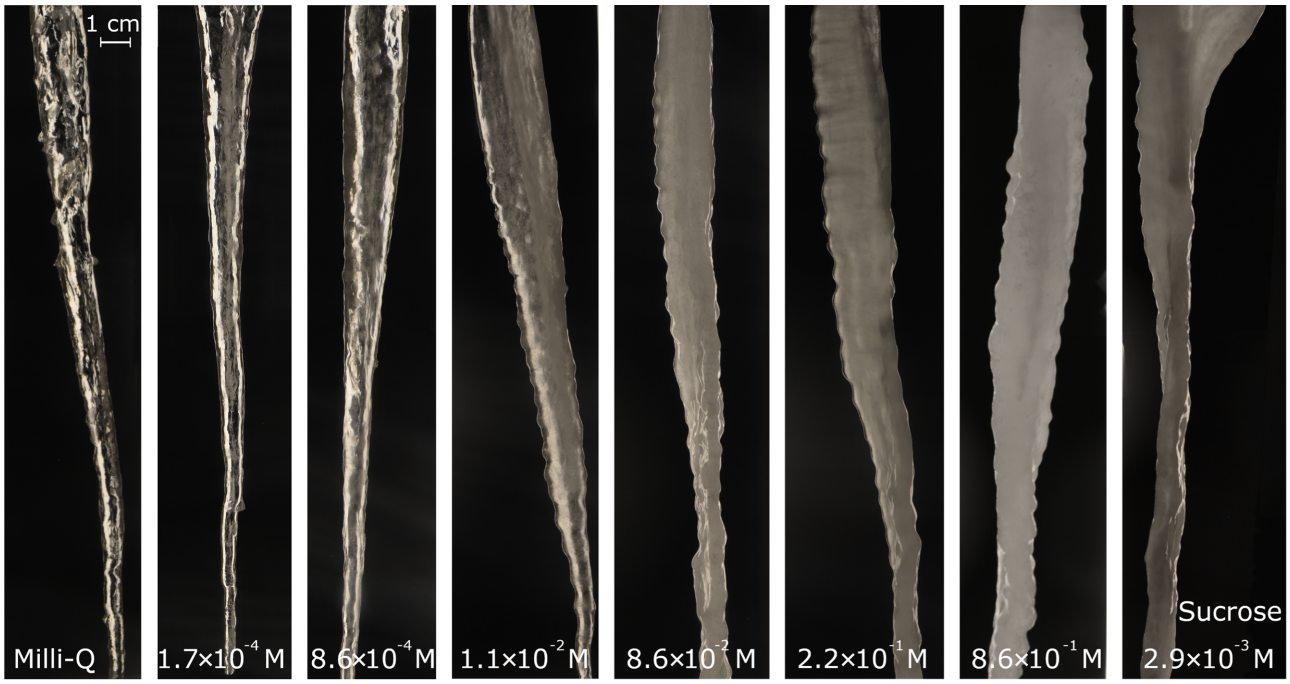

FIG. 2. Icicles grown from ultrapure water with added NaCl concentrations from 0 (left) to 0.86 M (right). Experiments are conducted in an ambient temperature of −15°C and the water temperature is approximately 15°C. In the first few minutes the water flow rate is slowly increased towards its final value of 60 ml/h. Ripple formation, opacity, and volume increases with salt concentration. The icicle on the right contains sucrose instead of NaCl.

In its most simple description, an icicle grows into a conelike contour with $W(t) \propto L(t)$. This is a linear approximation of the exact solution derived by Short and coworkers, who found a power-law relation $W' = L'^{3/4}$ for the dimensionless normalized shape; we find that in the length range investigated here, a simple linear approximation works quite well, and that we can model the scaled universal icicle shape as a cone. However, as shown in Fig. 3, this shape universality occurs only when impurities are present in the water. In this case, the icicle contours at different times can then be superimposed to one contour plot with the width and length normalized by $W(t)$ and $L(t)$, respectively. In Fig. 4 we show two typical examples of such superimposed icicle shapes (the shapes are symmetrical because they have been corrected for small overall bending of the icicle). As expected from the nonlinearity in Fig. 3, the experiment conducted with demineralized water [Figs. 4(a) and 4(b)] yields a poor collapse of data and deviates firmly from the perfect linear cone shape, depicted as the black dashed line. On the other hand, the experiment in which the water contains 8.5×10^{-2} Molar NaCl results in the predicted cone shape after normalization [Figs. 4(c) and 4(d)]. The blunt tip is due to the finite droplet size at the bottom of icicle. Comparing the two collapsed data sets also shows that ripple formation is enhanced by the presence of ionic impurities.

To investigate ripple formation in photographs such as those shown in Fig. 2 we extract contour plots and determine the coordinates of the rippled perimeter (Fig. 5). To identify the wavelength and amplitude of the ripples, we reconstruct the icicle profiles by a Fourier series containing the 100 lowest spatial-frequency components. In order to make a fair comparison between icicles of different lengths, we limit the Fourier analysis to the topmost 10 cm of the rippled edge. At a well-defined spatial frequency $k_{\max}$, we observe a peak, which can be fitted with a

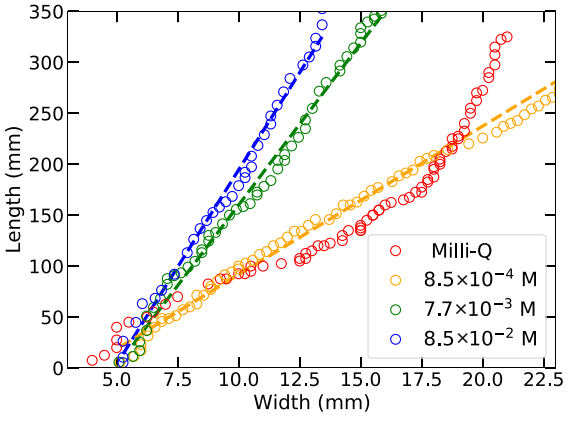

FIG. 3. Evolution of four icicles decomposed in total length (y axis) and measured maximum width close to the base (x axis). Icicles containing impurities follow a linear relation (dashed lines), whereas the icicle made of ultrapurified water does not.

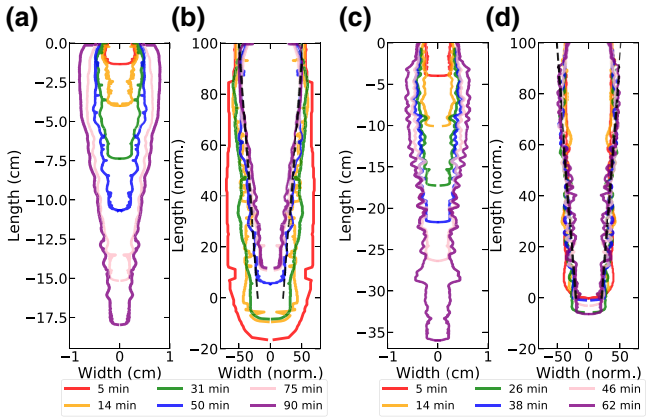

FIG. 4. Superimposed image of two icicles, normalized by its linear growth in time. The icicle on the left [(a),(b)] is made of ultrapurified water, the right icicle [(c),(d)] contains 8.5×10^{-2} M of NaCl. To correct for bending of the icicle shape we use the width instead of outer contour, which explains the symmetry in the figures. The black dashed lines depict the predicted linear cone shape. (a),(c) depict the situation before normalization as shown in (b),(d), respectively.

Gaussian function. The value of $k_{\max}$ corresponds to a ripple wavelength $\lambda = 2\pi/k_{\max}$. As a measure of the ripple amplitude, we use the maximum value of the Gaussian fit. In Fig. 5 we show a typical example of the data extracting procedure for an icicle with a NaCl concentration of $1.1 \cdot 10^{-2}$ M. The upper rippled 10 cm of Fig. 5(a) are extracted and plotted in Fig. 5(b). The Fourier spectrum with Gaussian fit of this particular region is displayed in Fig. 5(c). It yields a $k_{\max}$ of 7.3 cm^{-1}, corresponding to a wavelength 0.86 cm.

Figure 6 shows the ripple wavelength and amplitude as a function of salt concentration. The wavelength is independent of salt concentration, and we obtain a wavelength of $\lambda_{av} = 0.88 \pm 0.10$ cm for all salt concentrations, in agreement with the previous literature [2]. However, as can already been seen from direct visual observation, the ripple

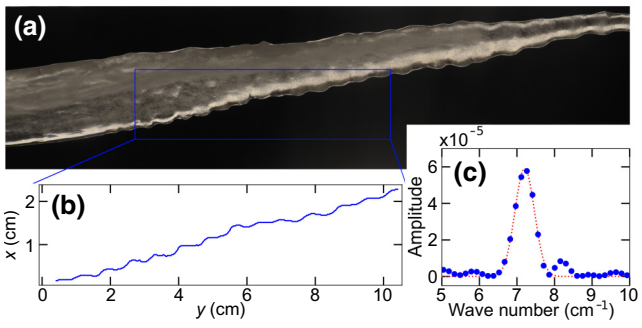

FIG. 5. Procedure to quantify ripple formation. (a) Photograph of an icicle with 1.1×10^{-2} M NaCl. (b) First 10 cm of the rippled edge corresponding to the area in (a) indicated by a blue box. (c) Corresponding Fourier spectrum with Gaussian fit.

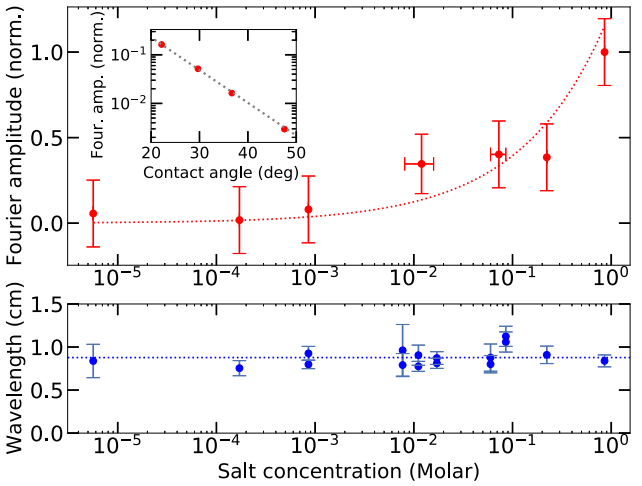

FIG. 6. Upper panel: normalized ripple amplitude dependence on salt concentration, as determined from Fourier spectra of icicle perimeters. Error bars are given by the standard deviation of the obtained amplitudes from experiments conducted at similar concentrations. Inset shows strong ripple amplitude dependence on measured contact angle. Red dotted line is the best fit of $A_{\text{norm}} = a\sqrt{C - C_t}$ with $a \approx 5/4$ and $C_t \approx 3.1 \times 10^{-18}$ M. Lower panel: ripple wavelength dependence on salt concentration. The blue dotted line indicates the average wavelength of 88 ± 10 mm, in agreement with the previous literature. Error bars indicate the full width at half maximum of the Fourier spectra.

amplitude increases drastically with salinity. These data indicate that the ripple amplitude is determined by a growing instability with salinity as its control parameter. To investigate this further, we test for which threshold salt concentration C_t the ripple amplitude A makes a transition from zero to nonzero, assuming the system undergoes a transition at this critical concentration. Using a mean-field approximation to model this transition, we expect an amplitude proportional to the square root of the control parameter, which here is the salt concentration [16]. Therefore, we fit the concentration-dependent amplitude data by

$$A(C) = a\sqrt{C - C_t}, \tag{1}$$

where C is the salt concentration, C_t its critical value, and a a concentration-independent scaling factor. From a least-squares fit, we find $C_t = 3.1 \times 10^{-18}$ M ≈ 0. From this result, we conclude that ripple formation occurs at all nonzero salt concentrations, and increases with the concentration of ionic impurities.

Further experiments show that the ripples are not dependent on the charge of the impurities: icicles grown from water containing sucrose instead of NaCl show similar ripple formation, as shown in the rightmost image of Fig. 2. Thus the impurities do not have to be ionic for ripple

formation to occur, as was suggested previously [8]. Furthermore, the sucrose solution conducts relatively poorly (3 μS/cm, 6 times larger than ultrapurified Milli-Q water), demonstrating that the electrical conductivity of solved ions also cannot be the origin of ripple formation.

In order to quantify the wetting behavior of ice, we conduct sessile droplet experiments close to the melting temperature. Droplets with similar impurity concentrations as the ice layers are brought into contact with the surface. Once an equilibrium is established we measure the contact angle, which is depicted as a function of ice temperature in Fig. 7. Close to the melting temperature, demineralized water from the Milli-Q system saturates at the frequently reported contact angle of 12°, indicated by the dashed horizontal line [17–20]. The presence of NaCl makes the contact angles collapse close to the melting temperature at approximately 5°, independent of the salt concentration. This is presumably caused by oversaturation of the ions at the surface due to brine rejection: there is no space for ions in the hexagonal lattice structure [21–23]. Hence, ions are rejected towards the solid-air interface when crystallization occurs, which also explains the increased opacity with impurity concentration (Fig. 2). This oversaturation depresses the melting temperature at the surface and therefore enhances the wetting of the top layer. We fit the contact angles θ based on Zisman's method, assuming a linear correlation between the surface tension of the liquid (γ_{lv}) and $1/\cos(\theta)$ [24,25]:

$$\frac{1}{\cos(\theta)} = a(C)\gamma_{lv} + b(C), \tag{2}$$

where the fitting parameters $a(C)$ and $b(C)$ are dependent on salinity C. As we assume that the contact angle is a result of a thermodynamic equilibrium with water in its supercooled liquid state, we use data from Hrubý *et al.* [26] to determine the surface tension of supercooled water. We find the following relation between surface tension and the temperature of undercooled water (see Figs. S3 and S4 within the Supplemental Material [27]):

$$\gamma_{lv} = -0.136\,T_k + 112.96, \tag{3}$$

with temperature T_k in kelvins. Combining Eqs. (2) and (3), we obtain the fits displayed in Fig. 7:

$$\theta = \cos^{-1}\left(\frac{1}{a(C)(-0.136T_k + 112.96) + b(C)}\right). \tag{4}$$

A closer inspection of the photographs such as shown in Fig. 2 reveals clearly distinguishable water droplets on the side of the smooth icicles sliding down with a stick-slip motion or in small rivulets. These sliding droplets are observed to have an advancing and receding contact angle of approximately 62° and 38°, respectively, at −15°C [leftmost panel in the figure, and more clearly visible in the red box of Fig. 8(a)]. This agrees very well with the measured contact angle on the flat surface, which is 47° at this temperature. Thus, the measured contact angle on the icicle agrees with the one on the flat surface, but does exhibit a significant contact angle hysteresis.

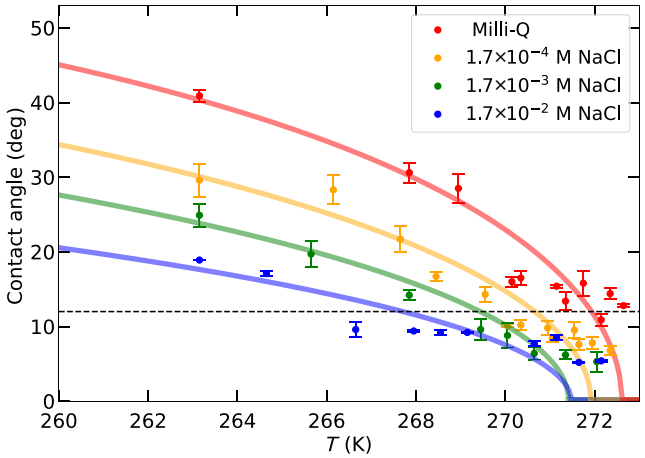

FIG. 7. Contact angle of 8-μl room-temperature water-sessile droplets containing various impurity concentrations deposited on planar ice made of an identical solution. Error bars indicate the standard deviation of five measurements. Slightly below the melting temperature, highly purified water displays an equilibrium contact angle of approximately 12° (dashed gray line). Ionic impurities lower the contact angle. Fits are to Eq. (2) using Eq. (3) from data by Hrubý *et al.* [26].

In contrast, the rippled icicles appear to be covered with a thin water film (middle panels), as is evident also from the visualization with the dye. We consequently do not observe any water droplets on these icicles, since all the water is in the film. Comparing to the contact angle measurements, this suggests that the water in this film contains more salt than the original solution, since part of the water has frozen onto the icicle. This difference confirms that the presence of small salt concentrations enhances the wetting of water on ice. As the salt concentration is not exactly known, it is difficult to make a detailed surface energy balance for the contact angle, as was done in Ref. [28]. Since the theories for the overall cone shape and the ripple formation are both based on the assumption of a thin liquid layer fully covering the icicle, the degree of wetting determines to what extent they are applicable. Correspondingly, the amplitude of the ripples increases strongly with decreasing contact angle (inset of Fig. 6). Thus wetting seems to be a key determinant for the shape of icicles.

In order to confirm this idea, we add methylene blue (Merck, 52015) to the water forming the icicles. This dye colors blue in a liquid water environment and turns to a transparent state once the water freezes. Therefore, it identifies the areas on the side of icicles that are covered by liquid water. In Fig. 8 we show a selection of

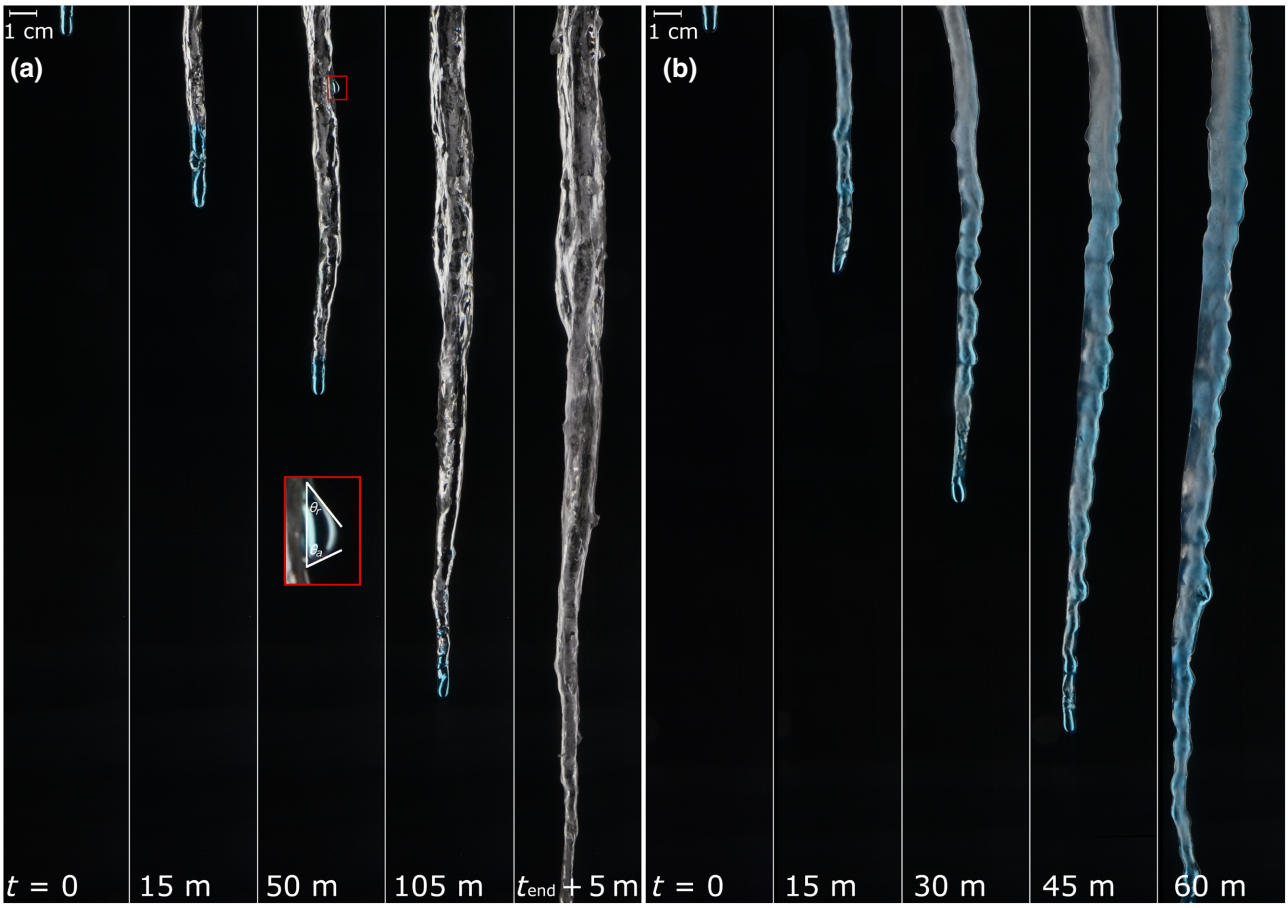

FIG. 8. Presence of liquid water around an icicle during growth at −15 °C from highly purified water (a) and water containing 8.6×10^{-2} M NaCl (b). The red box depicts a magnification of one droplet sliding down, which is used to analyze the advancing (θ_a) and receding (θ_r) contact angle. The water contained 2.5×10^{-5} M methylene blue in both experiments. This blue dye loses its color when trapped in a solid, therefore it exclusively accentuates the liquid areas on the icicle. Note that figure (a) is displayed on a nonlinear timescale, in contrast to (b). Hence, this emphasizes linear length growth in time for icicles containing solutes. $t_{end} = 160$ m.

time lapses of growing icicles. Figure 8(a) exclusively contains 2.5×10^{-5} M methelyene blue, thus no impurities are added. This results in a colorless icicle with a blue liquid tip and isolated blue droplets sliding down [see close up in the red box in Fig. 8(a)]. As a side note, the observation of a fully transparent blue-tipped icicle also contradicts previous claims about hollow icicle growth accompanied by an unfrozen interior [5,10,29]. In contrast, a similar experiment in the presence of 8.6×10^{-2} M NaCl is shown in Fig. 8(b). Herein, the blue color constantly covers a major part of the icicle, indicating that a thin liquid film is covering the surface.

The above analysis of icicles grown under identical circumstances from water with different impurity concentrations sheds light on the emergence of ripples. We find that the increase in ripple amplitude with impurity concentration is caused by changes in wetting of the icicle surface: the more salt is present, the lower the contact angle and the better, consequently, the wetting. As drops freezing on the surface cause the icicle shapes to be irregular, this means that the shape departs from the cone shape, and the ripples are not easily observable.

IV. CONCLUSION

Our results show that wetting of the liquid water on the ice surface plays a crucial role in the growth and morphology of icicles, and the apparent contradiction between the experiments by Morris and co-workers [8,9] (who found that ionic impurities are fundamental to ripple formation and icicle shape) and the theories of Short and Ueno [2,7] is solved by considering the impact of wetting on icicle growth. The presence of ionic impurities ensures complete wetting of the icicle surface, and as a consequence icicles that contain salt grow from a thin covering liquid film, as is assumed in the theories for icicle growth. On the other hand, icicles grown from purified water are not wetted by such a liquid film, but rather grow from individual droplets with stick-slip motion or from small rivulets. As a result,

icicles grown from pure water do not exhibit the instability of Ueno's theory, and thus do not have surface ripples. The same holds for the overall shape: when the icicle surface is not wetted, the thin-film fluid dynamics assumed in Short's theory does not occur, and the resulting icicle does not have the predicted universal conelike shape, but instead becomes similar to that of a drip candle.

ACKNOWLEDGMENTS

This work is financially supported by NWO Projectruimte Grant No. 680-91-133.

[1] K. Ueno, Pattern formation in crystal growth under parabolic shear flow. ii, Phys. Rev. E **69**, 051604 (2004).
[2] K. Ueno, Characteristics of the wavelength of ripples on icicles, Phys. Fluids **19**, 093602 (2007).
[3] K. Ueno, M. Farzaneh, S. Yamaguchi, and H. Tsuji, Numerical and experimental verification of a theoretical model of ripple formation in ice growth under supercooled water film flow, Fluid Dyn. Res. **42**, 025508 (2009).
[4] N. Maeno, L. Makkonen, K. Nishimura, K. Kosugi, and T. Takahashi, Growth rates of icicles, J. Glaciol. **40**, 319 (1994).
[5] L. Makkonen, A model of icicle growth, J. Glaciol. **34**, 64 (1988).
[6] K. Szilder and E. Lozowski, Simulation of icicle growth using a three-dimensional random walk model, Atmos. Res. **36**, 243 (1995).
[7] M. B. Short, J. C. Baygents, and R. E. Goldstein, A free-boundary theory for the shape of the ideal dripping icicle, Phys. Fluids **18**, 083101 (2006).
[8] A. S.-H. Chen and S. W. Morris, On the origin and evolution of icicle ripples, New J. Phys. **15**, 103012 (2013).
[9] J. Ladan and S. W. Morris, Experiments on the dynamic wetting of growing icicles, New J. Phys. **23**, 123017 (2021).
[10] N. Maeno and T. Takahashi, Studies on icicles. I. General aspects of the structure and growth of an icicle, Low Temp. Sci. **43**, 125 (1984).
[11] W. W. Mullins and R. Sekerka, Stability of a planar interface during solidification of a dilute binary alloy, J. Appl. Phys. **35**, 444 (1964).
[12] S. Chen, Ph.D. thesis, University of Oxford, 2019.
[13] S. Hardy and S. Coriell, Morphological stability of cylindrical ice crystals, J. Cryst. Growth **5**, 329 (1969).
[14] See Supplemental Material at http://link.aps.org/supplemental/10.1103/PhysRevApplied.19.024005 for details about the experimental setup.
[15] See Supplemental Material at http://link.aps.org/supplemental/10.1103/PhysRevApplied.19.024005 for experimental results of the length and width growth of icicles in time. When solutes are added, we observe a linear trend.
[16] Rizwan-uddin, Turning points and sub- and supercritical bifurcations in a simple bwr model, Nucl. Eng. Des. **236**, 267 (2006).
[17] C. A. Knight, The contact angle of water on ice, J. Colloid Interface Sci. **25**, 280 (1967).
[18] J. Drelich, E. Chibowski, D. D. Meng, and K. Terpilowski, Hydrophilic and superhydrophilic surfaces and materials, Soft Matter **7**, 9804 (2011).
[19] W. Ketcham and P. Hobbs, An experimental determination of the surface energies of ice, Philos. Mag. **19**, 1161 (1969).
[20] V. Thiévenaz, C. Josserand, and T. Séon, Retraction and freezing of a water film on ice, Phys. Rev. Fluids **5**, 041601 (2020).
[21] L. Vrbka and P. Jungwirth, Brine Rejection from Freezing Salt Solutions: A Molecular Dynamics Study, Phys. Rev. Lett. **95**, 148501 (2005).
[22] I. Gladich, W. Pfalzgraff, O. Maršálek, P. Jungwirth, M. Roeselová, and S. Neshyba, Arrhenius analysis of anisotropic surface self-diffusion on the prismatic facet of ice, Phys. Chem. Chem. Phys. **13**, 19960 (2011).
[23] I. Tsironi, D. Schlesinger, A. Späh, L. Eriksson, M. Segad, and F. Perakis, Brine rejection and hydrate formation upon freezing of NaCl aqueous solutions, Phys. Chem. Chem. Phys. **22**, 7625 (2020).
[24] D. Bonn, J. Eggers, J. Indekeu, J. Meunier, and E. Rolley, Wetting and spreading, Rev. Mod. Phys. **81**, 739 (2009).
[25] H. Fox and W. Zisman, The spreading of liquids on low energy surfaces. I. Polytetrafluoroethylene, J. Colloid Sci. **5**, 514 (1950).
[26] J. Hrubý, V. Vinš, R. Mareš, J. Hykl, and J. Kalová, Surface tension of supercooled water: No inflection point down to –25°C, J. Phys. Chem. Lett. **5**, 425 (2014).
[27] See Supplemental Material at http://link.aps.org/supplemental/10.1103/PhysRevApplied.19.024005 for detailed information about the data that is used to create the fit in Fig. 7.
[28] J. D. Smith, R. Dhiman, S. Anand, E. Reza-Garduno, R. E. Cohen, G. H. McKinley, and K. K. Varanasi, Droplet mobility on lubricant-impregnated surfaces, Soft Matter **9**, 1772 (2013).
[29] R. Laudise and R. Barns, Are icicles single crystals?, J. Cryst. Growth **46**, 379 (1979).